Table of Graphical Contents

Depth Dependent Nanomechanical Analysis of Extracellular Matrix in Multicell Spheroids.

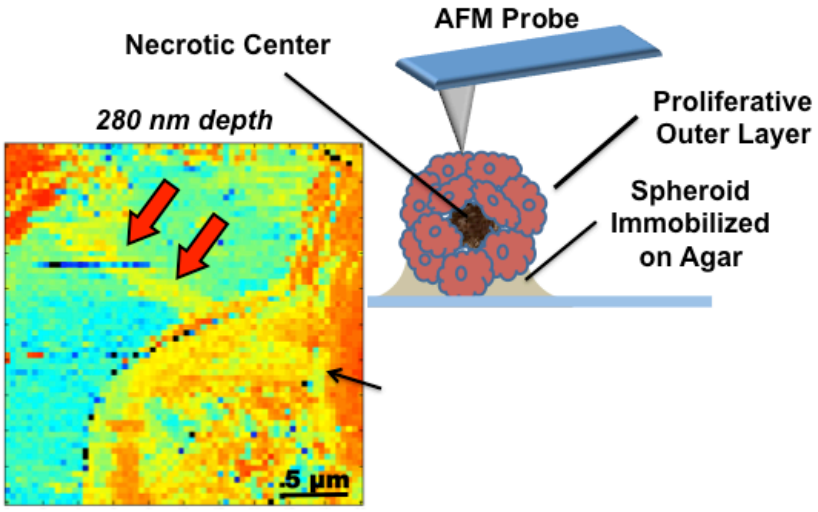

Most tumor dissolving drugs are aimed to penetrate to outer most proliferative layer in a multicell spheroid. Nanomechanical investigation with Atomic Force Microscope has revealed new details regarding various nanomechanical heterogeneities when cells are embedded in extracellular matrix in Multicell spheroidal culture. This investigation sheds new insight into growth mechanics of tumors in in-vivo & in-vitro environment.

Depth Dependent Nanomechanical Analysis of Extracellular Matrix in Multicell Spheroids.

Varun Vyas[1,4(✉)], Melani Solomon[2,3], Gerard G.M. D'Souza[2], Bryan D. Huey[1(✉)]

[1]Materials Science and Engineering Department, University of Connecticut, Storrs, CT 06269, United States

[2] Pharmaceutical Sciences, Massachusetts College of Pharmacy & Health Sciences, Boston, MA 02115, United States

[3]McKusick-Nathans Institute of Genetic Medicine, Johns Hopkins University, Baltimore, MD 21205, United States

[4]Department of Physics and Astrophysics, University of Delhi, Delhi – 110007, India

[1]**Mailing Address:** Department of Materials Science & Engineering

97 North Eagleville Road, Unit 3136

Storrs, CT 06269-3136

Office: IMS-158

Phone:(860) 486 3284

(✉) **Email**: varun.shiva@gmail.com

(✉) **Email**: bryan.huey@uconn.edu

Email: melani.the.piscean@gmail.com

Email: gerard.dsouza@mcphs.edu

Abstract

Nanotechnology has revolutionized the field of cancer biology and has opened new avenues towards understanding nanomechanical variations in rapidly growing tumors. Over the last decade Atomic Force Microscope (AFM) has played an important role in understanding nanomechanical properties of various cancer cell lines. This study is focused on Lewis Lung Carcinoma Cell (LLC) tumors as 3D multicell spheroid (MCS). Such multicell structures have enabled investigation of various components of tumors *in-vitro*. To better comprehend mechanical properties of cells and its surrounding extracellular matrix (ECM), depth dependent indentation profiling (DDIP) was performed with Atomic Force Microscope (AFM). Force volume based force-vs-indentation curves were used to create stiffness profiles at various depths. AFM investigations of sample MCS-1 & MCS-2 revealed three nanomechanical topographies, Type A-collagen stress fibers, Type B-high stiffness at cell membrane - ECM interface and Type C – identification of cell lying deep inside matrix at the a depth of 1.44 microns. High stiffness of both Type A and Type B features in ECM acts as a controlling factor towards delivery of therapeutics from proliferation zone to quiescent zone in a MCS. Various nanomechanical heterogeneities revealed in this investigation can shed new light in developing correct dosage regime various tumor dissolving drugs and designing more controlled artificial extracellular matrix systems for replicating tissue growth in-vitro.

KEYWORDS

AFM, Nanomechanics, Spheroids, Lewis Lung Carcinoma, Extracellular Matrix

Depth Dependent Nanomechanical Analysis of Extracellular Matrix in Multicell Spheroids.

Introduction

Tissues in higher living organisms have multilayered cell-cell and cell-extracellular matrix (ECM) interactions. Culturing of 3D cell cultures known as Multicell Spheroids (MCS), have become a preferred means to study and simulate an in-vivo environment[1]. 3D cell cultures with resembling structural and functional properties to real tissues has helped in understanding growth of tumorous, effects and penetration of toxins within a tissue and developing targeted drug-delivery systems[2–4].

With the discovery of ECM in MCS gave us better understand towards developing 3D cell cultures[5]. Matrix act as both mechanical and biochemical shield that protects a cell. ECM also works as an information gateway systems that allows selective passage of signals via cell membrane. Here composition of ECM was found similar to that of tumors *in vivo.* Fibronectin, laminins, proteoglycans and collagen form major structural components within the matrix[5,6]. Structural forming elements like collagen and laminins play a major role in giving stability to MCS.

MCS being a tumor analog have inherent gradient of nutrients, oxygen and metabolites. In rapidly growing cultures, they have central necrotic core which is surrounded by layer of quiescent viable cells and an outer most layer of rapidly proliferating cells. Central necrotic core and region of hypoxia is critical for testing anti-cancer therapeutics. Hypoxia have been identified as one of the cause of drug resistance in tumors[7–9]. Here penetration of drug through various layers of MCS becomes a limiting factor towards drug efficacy. Therefore, this

investigation is aimed towards understanding nanomechanical properties at surface of the spheroid where along with the cells, large volume of ECM is present that encapsulates multicellular structure. By measuring its stiffness one can look for better means to dissolve outer mass of cells and develop methods to deliver therapeutics into the quiescent zone for complete dissolution of the multicell structure[2].

In this study, spheroidal cell cultures were developed with lewis lung carcinoma (LLC) cell line. LLC cell lines were derived from carcinoma of lung of a C57BL mice. LLC cells have been used to determine outcome of drug induced toxicity by chemotherapeutic agents, developing methods to suppress metastasis, etc.[10,11]. There are number of methods like spinner flask, hanging drop, etc. that are being used to developing spheroidal cell cultures[1]. For the current investigation LLC cell spheroids were developed with liquid overlay method[12].

Objective of this communication is to highlight variations in stiffness of ECM, cells and specifically at ECM-cell membrane interface. It is at the membrane where stiffness of the matrix limits the penetration of the therapeutic agents. ECM is equally distributed within proliferation zone and quiescent zone. Hence the stiffness (i.e high density of ECM components) at the cell surface can be a controlling factor towards drugs penetration. To map differential nanomechanics at the MCS surface, force volume measurements were conducted with help of atomic force microscope (AFM). Various other applications of AFM in the field biomaterials and cell biology include probing of biocompatible nature of metal oxide surface[13–15], nanostethoscopy of cardiomyocytes and other living organisms[16–18], Cell Nanomechanics[19–21], etc.

In order to understand nanomechanical properties of speheroid, depth dependent indentation profiling (DDIP) of cells and surrounding ECM can reveal minute changes in stiffness as a function of depth[22]. Indentation dependent profiling methods have been explored by number

of researcher in the field of AFM biology. Measurements conducted by *Rico et al* and similar groups primarily measure modulus at one data point at time along the length of the force curve[23–25]. In this investigation, successive segments of Force-vs-distance curve were analyzed that provided 'step-wise-modulus' that helps in detecting variations in stiffness in 3-dimensions.

Error parameters associated with local mechanical properties were also used in analysis. It helped to identify small jitters experienced by AFM probe as it indents into a cell having well defined membrane as compared to ECM which is highly viscous mass of proteins, glycoproteins, etc. In our previous investigation with agarose gels, one could observe that stiffer gels had narrow error distribution when compared with agarose gels having lower stiffness[22].

DDIP measurements were conducted using pyramidal AFM probe. As probe indents directly into viscous mass of ECM surrounding cells, it forms a conical indent at the point of contact. Due to square pyramidal geometry of the probe, modulus for developing indentation profile was calculated using Sneddon's model.

$$\boldsymbol{F_{model} = C_{model} E^{*} \delta^{n_{model}}} \qquad (1)$$

$$\boldsymbol{C_{Sneddon} = \frac{2}{\pi} \tan \alpha\,, \qquad n_{Sneddon} = 2} \qquad (2)$$

$$\boldsymbol{\frac{1}{E^{*}} = \frac{1 - \nu_{tip}{}^{2}}{E_{tip}} + \frac{1 - \nu_{sample}{}^{2}}{E_{sample}} \approx \frac{1 - \nu_{sample}{}^{2}}{E_{sample}}} \qquad (3)$$

$$\mathbf{E}^* = \frac{\left\{\frac{\partial\left[\left(\mathbf{F}_{model}\right)^{1/n}\right]}{\partial\delta}\right\}^n}{\mathbf{C}_{Sneddon}} \tag{4}$$

$$\mathbf{slope}_{std} = \sqrt{\frac{\frac{1}{j-2}\sum_{i=1}^{j}\left[\left(\mathbf{F}_{model}\right)^{1/n_i} - \left(\mathbf{F}_{ideal}\right)^{1/n_i}\right]^2}{\sum_{i=1}^{j}\left(\delta_i - \overline{\delta}\right)^2}} \tag{5}$$

A simplified equation of measured force ($\boldsymbol{F_{model}}$) vs indentation to a model-dependent power ($\boldsymbol{\delta^n}$) curves is shown as Equation-1. Other terms of the equation include a model dependent constant term ($\mathbf{C}_{\boldsymbol{model}}$), and the local reduced modulus (**E***). Equation for Sneddon's mechanics and reduced modulus (E*) are presented as Equation 2 & 3 respectively. For calculating reduced modulus, Poisson ratio ($\boldsymbol{\nu}$) of 0.3 was employed for all samples. Modulus (E) of the tip is >100 GPa as compared to sample's < 1MPa. Hence, the first term in Equation 3 becomes negligible and is dropped from the final equation.

The local reduced modulus for any given Force-vs-indentation curve was calculated from slope of the nth root of the curve, all is taken to the nth power and is divided by the appropriate constant (Equation 4). This approach towards calculating the modulus also provides standard deviation of the modulus. Here standard deviation of the slope is calculated by simple linear regression in Equation 5 and is substituted by standard deviation of the actual slope in Equation 4(braces). Effective local modulus and its standard deviation for every depth and every pixel was calculated using Equation 3. Error maps developed here can used to interpret indentation data from novel perspective.

Earlier AFM measurements by Plodinec *et al* on rat spheroids were only focused on differential nanomechanical properties at the core and periphery of the tumorous structure[26]. This study is an attempt to further explore nanomechanics of MCS by mapping stiffness of cells and surrounding ECM. Indentation profiling of sample MCS-1 and MCS-2 over 20 micron sized area has brought forth three nanomechanical topographies into obervation, Type –A i.e. stiffness of long range Collagen I stress fibers, Type- B i.e. high stiffness at interface of cell membrane & ECM, and Type-C i.e. indentation mapping up to depth 1.35 µm has also revealed stiffness of cells lying deep inside ECM. Modulus mapping of MCS will help to develop effective drug delivery systems that can by penetrate ECM coating and other surrounding tissue around the tumor.

Material and Methods

Production of spheroids:

Lewis lung carcinoma (LLC) cells were obtained from ATCC (Manassas, VA). LLC cells were maintained in Dulbecco's modified Eagle media (DMEM, Corning cellgro®, Manassas, VA) supplemented with 10% fetal bovine serum and 1% penicillin-streptomycin. Spheroids were produced using a liquid-overlay technique on agar surfaces. Briefly, 1% agar was coated in each well of a 96-well plate. Following the solidification of agar, 1000 LLC cells were plated in each well and the plate was centrifuged using a plate centrifuge (ThermoFisher Marathon 3000R) at 250xg for 15 min. The plate was placed in 5% CO_2, 37°C atmosphere and the spheroids were allowed to grow for 6 days.

After 6 day of incubation spheroids were fixed on the glass coverslip using agarose gel. 0.1 % of warm agarose gel was allowed to cool down at room temperature and is gently poured over the

coverslip. Before complete solidification of gel, a spheroid is carefully pipetted on its surface and lower half of the spherical mass of cell gets immobilized over the agar surface

Nanomechanical Measurements

AFM based force mapping measurements were conducted with an Asylum Research MFP-3D AFM with integrated inverted optics (Nikon TE-2000), in a liquid cell for complete immersion during the experiments. Arrays of 64 x 64 force indentations were acquired over a 20 μm x 20 μm area. All force maps were collected with indentation velocities of 32 μm/sec, amounting to individual indentations at a rate of ~2 Hz. Spring constants of the Olympus TR800PB probes used throughout were calibrated following the widely applied Sader method[27] . Sneddon derived stiffness as a function of depth, as well as novel maps of the error in these calculations, were performed using custom analytical and visualization routines written with Matlab software.

Results & Discussion

Spheroids were initially regarded as simple aggregates of cells with intimate cell-to-cell contacts. It was with discovery of ECM it became clear how closely they resembled tumors *in-vivo*(5). Over the years as the understanding of ECM in spheroids became better, some groups have started to develop permissive hydrogels that mimic ECM in MCS. They have tried to substituting protein based ECM components with poly(ethylene glycol) (PEG)[28–30]. Such artificial matrices can only act as a physical scaffold to hold cells proliferating in a 3-dimension. But the exact nanomechanical properties in a native ECM environment is controlled by collagen, laminins and other components. Tissues engineered with artificial ECM can have different

mechanism towards delivery of therapeutics and nutrients in 3D cultures. Therefore, information gather via nanomechanical investigation of matrix and cells in a MCS can help in improving hydrogel based replacements for ECM.

To best understand nanomechanics of spheroids, measurements were conducted over 20 micron sized area. 20 spheroids were examined to get most appropriate spot that presents both ECM and cells adjacent to each other. Each data set contains 4096 force-vs-indentation curves. Measurements were conducted at individual indentation rate of ~ 2 Hz. It is a known fact that the measured mechanical stiffness depends on the loading rate[23,19]. This investigation required examining large number of samples, which in turn produced large volumes of data for analysis. Thus, in order to accelerate the experimental procedures and maintain viability of cells under the AFM probe, experiments were performed at a high indentation rate (~ 2 Hz). At lower rates, duration each scan becomes to long, this may kill or damage structural integrity MCS under investigation. Therefore, the stiffness maps presented in this article, should be used to appreciate relative differences in stiffness between cells and ECM within a single data set.

To determine the point of contact with the sample, relatively high contact force of 4 nN was considered. At such high contact force there is sufficient deformation of cell around the AFM probe which has been predicted[31,32] and observed[33] by various research groups. This study presents data from two LLC spheroids, MCS-1 and MCS-2. Implementation of DDIP on MCS-1 is shown in Figure 1. Data from each indentation curve is split into small fragments and each fragment is fitted with Sneddon's model to estimate stiffness at certain depth as illustrated in Figure 1a.

Measured stiffness at depth of interest is plotted in form of a stiffness map as shown in Figure 1b. Stiffness map presented here is at depth of ≤ 80 nm. 64 x 64 nanoindentations in each data

set has considerably high resolution to differentiate cells from ECM. Illustration Figure 1c shows various features observed in figure 1b. Yellowish central region, green in Figure 1c is identified as ECM. Spheroid suspended in growth media (DMEM) will continuously dissolve some of its matrix components into the surrounding aqueous environment. This creates large variations in stiffness at depths closer to surface of the spheroid. Therefore, ECM in Figure 1b at ≤ 80 nm depth, there is large variation is modulus starting from 3 kPa and going upto 300 kPa. To get maximum contrast, color bar for the modulus is presented in log scale. Here presentation of the modulus in logarithmic scale simplifies identification of minute features having stiffness unlike rest of the matrix. Error indentation profiles at ≤ 80 nm can be studied from Figure 4a. Due to lack of clearly defined structures or membrane over ECM standard deviation of the calculated modulus (percentage error) is greater than 1. Whereas due to presence of cell membrane, percentile error is comparatively lower.

Cells in Figure 1b are observed in lower right and upper left corner on the image. At depth of 80 nm, probe has just indented into cells membrane. When compared to ECM they have relatively higher stiffness. On closer observation one can identify three different cells that are embedded in ECM. Modulus of all the cells > 100 kPa and goes upto 300 kPa. Further analysis of MCS-1 at depths of 280 nm, 800 nm, 1 μm and 1.35 μm is shown in Figure 2. On comparing indentation profile in Figure 1b at ≤ 80 nm with Figure 2a at depth of 280 nm, one can observe overall decrease in modulus as probe indents deeper into cells and adjacent matrix. Modulus of the bulk of the matrix has gone down to 10 kPa and that of cells embedded in the ECM have stiffness between 30 kPa to 100 kPa. This decrease in modulus at shallower depths, highlights one the advantages of using DDIP for investigating complex biological surfaces. As square pyramidal probe indents deeper into the surface, any local variations in stiffness are instantaneously

recorded in a force-vs-indentation curve. Stiffness maps from sample MCS-2 shows similar trend (Figure 5). Stiffness of both matrix and cells gradually decrease from 0.17 nm to 1.44 μm. Features observed in MCS-2 are described with help of illustration Figure 5a.

Closer inspection of indentation profiles of both MCS-1 and MCS-2 brings forth certain features which otherwise may not be visible when whole curve is subjected to one single fit. Depth dependent approach to measure stiffness of the surface of spheroids has helped in identifying three nanomechanical topographies, Type A, Type B & Type C. These features are explained by illustration in Figure 3. Type A structures look like elongated fibrillary structures. They are possibly collagen based stress fibers that help cells to mechanically sense and respond to the presence of other cells over long distances (~ 100 μm).

Collagen of types I, II III, V and XI are fibril-forming collagens[34]. It is reported that when hMSCs are grown on type-1 collagen gels, they appear to respond to stiffness of glass slide via 1000 μm of collagen gel[35]. Fibroblast grown with fibrin gels can sense presence of other cells up to 250 μm away and are also known to respond by aligning themselves relative to each other[36]. Therefore, stiffness and stability of MCS can be directly correlated to modulus of these stress fibers. Collagen fibers are known to have modulus greater than 0.3 GPa but can have lower stiffness depending on the source of the biomaterial[37–40]. Stiffness of bulk ECM and cells is around few 10s of kilo Pascals, Hence presence of any type I collagen fibers should have stiffness greater than rest of biological material forming a MCS. From the indentation profiles presented in this investigation, features similar to stress fiber can be observed in Figure 2a & 5c are marked by red arrow. Collagen fiber in MCS-2 are also depicted in illustration of indentation maps shown in Figure 5a.

In Figure 1b, stress fiber identified in Figure 2a looks like a smear in the center of the matrix. Its stiffness up to depth of 80 nm is ≥ 100 kPa. Collagen fibers have high stiffness but due its presence close to surface of ECM it got masked by high degree of variability in modulus at the surface of spheroid. At depth of 280 nm (Figure 2a) it can be observed as an interconnecting fiber between cells separated by distance of 10 microns. It has been reported that collagen fibers can have diameter greater than 250 nm and sometime they might be as thin as 30 nm[41,42]. A very high stiffness among collagen fiber can also be observed from Figure 5 at depths of 0.49 µm, 0.8 µm, 1 µm and 1.44 µm. Pixel along the length of the fiber have black contrast, denoted as NaN in stiffness and error maps. Here pixels having modulus greater than 316 kPa are shown with a black contrast. As the probe travels deeper into the surface, modulus observed directly correlates with the resistance offered by collagen fiber during the downward penetration of the probe into the ECM. Figure 5b at depth of 0.17 µm has average stiffness of the fiber is 10 kPa but it gradually increases at shallower depths. Accurate estimation of modulus of stress fiber in MCS will also depend on the loading rate, plus fibers are spread across a squishy matrix of biomolecules. Fibers will get pulled and pushed around as probe indents into the spheroids. Hence, stress and strain factors will also come into play for more precise measurement of modulus of collagen fibers in 3D cell cultures[43].

Type B nanomechanical topographies are indicative of interactions taking place between ECM and cell membranes. When cells are grown as monolayered cultures, apical surface is exposed to aqueous media whereas *in-vivo* most cells are embedded in ECM. Cells associated with fluid connective tissues like blood and lymph can be found floating or exposed to aqueous environment. Therefore, nanomechanical properties and passage of nutrients via cell membrane depends on its interaction with surrounding matrix. In this investigation it was interesting to

observe that where cell membrane was in direct contact with ECM, a very high modulus ≥ 300 kPa was observed. Illustration in Figure 3-(B) describes point of interaction between cell membrane and ECM. As the probe indents into the membrane-matrix interface (MMI) there is a sharp increase in stiffness. Regions of high stiffness at MMI are marked by green arrows in Figure 2b & 2c at depth of 800 nm & 1 µm respectively and in Figure 5c at depth of 0.49 µm.

Effects of MMI can also be observed in percentage error profiles in Figure 4c. At depth of 1 µm, MMI regions have higher percentage errors going up to 10 units, marked by green arrows. In sample MCS-2 at depth of 0.17 µm (Figure 5b) MMI has stiffness > 100 kPa. Top most cells on the surface of MCS have layer of ECM over them. As AFM probe approached from the surface whole top surface of the cell should have higher stiffness as compared to rest of the cell body. This effect can be observed in Figure 1b (depth $\leq$ 80 nm) where cells on the lower right and top left corner have modulus > 100 kPa and at some place it goes up to 300 kPa. Hence, the regions of higher modulus at MMI can be found at the apical surface (Figure 1b) as the whole cells are embedded in ECM and on the edges as marked by green arrows in Figure 3b,3c & Figure 5b.

This increase in stiffness at MMI can be attributed to formation of basal lamina assembly at the cell surface[44]. As long range stress fiber are Collagen I fiber, ECM architecture near the cell surface is composed interconnected polymers of Collagen IV and VII[45]. They are bound to the laminin sheets which are organized on the cell membrane by integrins and dystroglycan. Binding of collagen IV network to laminin takes place via nidogen molecules[46]. Assembly is further strengthen by binding to Collagen VII dimers[6,47,48]. A conclave of structural proteins over the cell membrane strengthens basal lamina. This can considerably increases modulus of the cell membrane above 100 kPa. Therefore, cells embedded in ECM around spheroids have shell like structure around them that provides them lot of mechanical stability.

The last nanomechanical topography i.e. Type C marked by red square in Figure 2d can only be observed in MCS-1. Outer surface of spheroid doesn't have an even distribution of cells. There are gaps filled with viscous ECM. As probe indents into ECM there is a decrease in stiffness from the depth of ≤ 80 nm (Figure 1b) to 280 nm (Figure 2a). Average stiffness of the ECM goes down from 31.6 kPa to 10 kPa. Only collagen fiber marked by double red arrows has stiffness higher than the surrounding ECM. Thereafter from 800 nm (Figure 2b), 1 µm (Figure 2c) and 1.35 µm (Figure 2d), one can observe a gradual increase in stiffness, going up to 100 kPa. This gradual increase in stiffness of ECM is explained in Figure 3 as Type C nanomechcanical topography. This increase of stiffness can be attributed to a cell underlying deep inside the ECM. On closer examination of error profile in Figure 4, from ≤ 80 nm to 500 nm error decreases to 0.01 units but at 1 micron depth regions having stiffness >0.1 unit. This can be due to the fact that MMI has stiffness greater than that of cell and ECM.

This observation of Type C features is limited by length of the AFM probe. Olympus TR800PB probes have height of 3 microns and analysis of data is limited to depth of 1.5 microns. ECM being highly viscous, it tends to adhere to AFM probe. Therefore after extensive number of experimental trials, indentation of the probe was limited to depth of 2 micron. Beyond the depth of 2 µm probability of contamination probe became very high. Hence investigating of nanomechanical properties of cells in quiescent zone of the spheroid will require development of specialized AFM probes.

Main objective of culturing MCS is to replicate tumorous environment *in-vitro* for developing therapeutics that can penetrate and kill any cancerous growth inside the human body. Due to layered structuring and compactness of tumors, breaching out most layer of cells including targeted drug delivery of drug becomes a limiting factor towards curing a cancer patient. ECM in

tumors is known to present a transport barrier that restrict drug penetration inside a solid tumor. Treatment of collagenase prior to delivery of 100 nm sized nanoparticles has found to increase particle penetration by 4-fold[49]. Both Type A & B topographies are collagen based. Collagenase treatment when coupled with nanomechanical studies can help in building correct dosage regime. Drugs similar to collagenase cannot be directly released into the system, they too have to be targeted towards disease tissue.

Understanding tumor microenvironment plays a crucial role in developing effective anticancer drugs[4]. Composition of ECM in MCS is considerably different when compared with monolayer cultures[50]. Previous studies have also suggested increased stiffness of ECM in malignant phenotypes/cultures and is associated with increased concentration of type I collagen in the matrix[51–53]. Plus type IV collagen being most abundant constituent of basement membrane, is associated with tumor fibrosis and accumulates in tumor interstitium[47,54,55]. Therefore, detection of high stiffness at MMI by AFM probe is consistent with studies conducted on ECM and tumorous tissues so far. With DDIP, scanning surfaces of the cultures with artificial ECM would help fine tune nanomechanics in 3D cell cultures.

Conclusion

With recent developments in AFM and force volume imaging, implementation DDIP to understand nanomechanics of 3D cultures and tumorous tissues can become a common procedure in cancer biology. Detection of other nanomechanical topographies deep inside 3D cultures can also be performed by developing specialized AFM probe that have height greater than 3 micron.

Due to the opaque nature of the spheroid it was not possible to conduct simultaneous fluorescence imaging. But with the development of Light-sheet-based fluorescence microscopy[56], one day it might be possible to combine two techniques that would give us fine control to probe and selective study mechanical properties of cells in proliferation and quiescent zone in MCS.

Funding

VV and BDH acknowledge the University of Connecticut's Institute of Materials Science and NSF Nano-Bio-Mechanics grant 0626231.

Author Contributions

All authors have given approval to the final version of the manuscript.

Notes

Authors declare no competing financial interests.

References:

[1] R.-Z. Lin, H.-Y. Chang, Recent advances in three-dimensional multicellular spheroid culture for biomedical research, Biotechnol. J. 3 (2008) 1172–1184. doi:10.1002/biot.200700228.

[2] G. Mehta, A.Y. Hsiao, M. Ingram, G.D. Luker, S. Takayama, Opportunities and challenges for use of tumor spheroids as models to test drug delivery and efficacy, J. Control. Release. 164 (2012) 192–204. doi:https://doi.org/10.1016/j.jconrel.2012.04.045.

[3] S.H. Jang, M.G. Wientjes, D. Lu, J.L.-S. Au, Drug Delivery and Transport to Solid Tumors, Pharm. Res. 20 (2003) 1337–1350. doi:10.1023/A:1025785505977.

[4] A.I. Minchinton, I.F. Tannock, Drug penetration in solid tumours, Nat Rev Cancer. 6 (2006) 583–592. http://dx.doi.org/10.1038/nrc1893.

[5] T. Nederman, B. Norling, B. Glimelius, J. Carlsson, U. Brunk, Demonstration of an Extracellular Matrix in Multicellular Tumor Spheroids, Cancer Res. 44 (1984) 3090 LP-3097. http://cancerres.aacrjournals.org/content/44/7/3090.abstract.

[6] J.K. Mouw, G. Ou, V.M. Weaver, Extracellular matrix assembly: a multiscale deconstruction, Nat. Rev. Mol. Cell Biol. 15 (2014) 771–785. doi:10.1038/nrm3902.

[7] S.-H. Kim, H.-J.K. and C.R. Dass, The Reciprocal Interaction: Chemotherapy and Tumor Microenvironment, Curr. Drug Discov. Technol. 8 (2011) 102–106. doi:http://dx.doi.org/10.2174/157016311795563875.

[8] F. Andre, N. Berrada, C. Desmedt, Implication of tumor microenvironment in the resistance to chemotherapy in breast cancer patients, Curr. Opin. Oncol. 22 (2010) 547–551.

[9] M. PV Shekhar, Drug resistance: challenges to effective therapy, Curr. Cancer Drug Targets. 11 (2011) 613–623.

[10] J.S. Bertram, P. Janik, Establishment of a cloned line of Lewis lung carcinoma cells adapted to cell culture, Cancer Lett. 11 (2017) 63–73. doi:10.1016/0304-3835(80)90130-5.

[11] M.S. O'Reilly, L. Holmgren, Y. Shing, C. Chen, R.A. Rosenthal, M. Moses, W.S. Lane, Y. Cao, E.H. Sage, J. Folkman, Angiostatin: A novel angiogenesis inhibitor that mediates the suppression of metastases by a lewis lung carcinoma, Cell. (1994). doi:10.1016/0092-

8674(94)90200-3.

[12] J. Carlsson, J.M. Yuhas, Liquid-overlay culture of cellular spheroids., Recent Results Cancer Res. (1984). doi:10.1007/978-3-642-82340-4_1.

[13] S. Kessel, S. Schmidt, R. Müller, E. Wischerhoff, A. Laschewsky, J.-F. Lutz, K. Uhlig, A. Lankenau, C. Duschl, A. Fery, Thermoresponsive PEG-Based Polymer Layers: Surface Characterization with AFM Force Measurements, Langmuir. 26 (2010) 3462–3467. doi:10.1021/la903007v.

[14] K.D. Jandt, M. Finke, P. Cacciafesta, Aspects of the physical chemistry of polymers, biomaterials and mineralised tissues investigated with atomic force microscopy (AFM), Colloids Surfaces B Biointerfaces. 19 (2000) 301–314.

[15] V. Vyas, A. Podestà, P. Milani, Probing Nanoscale Interactions on Biocompatible Cluster-Assembled Titanium Oxide Surfaces by Atomic Force Microscopy, J. Nanosci. Nanotechnol. 11 (2011) 4739–4748. doi:10.1166/jnn.2011.4113.

[16] A. Keaton, J.F. Holzrichter, R. Balhorn, W.J. Siekhaus, Nanostethoscopy: A New Mode of Operation of the Atomic Force Microscope BT - Forces in Scanning Probe Methods, in: H.J. Güntherodt, D. Anselmetti, E. Meyer (Eds.), Springer Netherlands, Dordrecht, 1995: pp. 91–97. doi:10.1007/978-94-011-0049-6_8.

[17] V. Vyas, N. Nagarajan, P. Zorlutuna, B.D. Huey, Nanostethoscopy: Atomic Force Microscopy Probe Contact Force versus Measured Amplitude of Cardiomyocytic Contractions, J. Bionanoscience. 11 (2017) 319–322.

[18] I. Sokolov, Toward the nanoscale study of insect physiology using an atomic force microscopy-based nanostethoscope, MRS Bull. 37 (2012) 522–527.

[19] I.D. Medalsy, D.J. Müller, Nanomechanical Properties of Proteins and Membranes Depend on Loading Rate and Electrostatic Interactions, ACS Nano. 7 (2013) 2642–2650. doi:10.1021/nn400015z.

[20] S.E. Cross, Y.-S. Jin, J. Rao, J.K. Gimzewski, Nanomechanical analysis of cells from cancer patients, Nat. Nanotechnol. 2 (2007) 780–783. http://dx.doi.org/10.1038/nnano.2007.388.

[21] Y.F. Dufrene, D. Martinez-Martin, I. Medalsy, D. Alsteens, D.J. Muller, Multiparametric imaging of biological systems by force-distance curve-based AFM, Nat Meth. 10 (2013) 847–854. doi:10.1038/nmeth.2602.

[22] V. Vyas, M. Solomon, G.G.M. D'Souza, B.D. Huey, Dynamic and Depth Dependent Nanomechanical Properties of Dorsal Ruffles in Live Cells and Biopolymeric Hydrogels,

J. Nanosci. Nanotechnol. (In Press) (2018). doi:https://doi.org/10.1101/189852.

[23] Y.M. Efremov, A.A. Dokrunova, D. V. Bagrov, K.S. Kudryashova, O.S. Sokolova, K. V. Shaitan, The effects of confluency on cell mechanical properties, J. Biomech. (2013). doi:10.1016/j.jbiomech.2013.01.022.

[24] F. Rico, P. Roca-Cusachs, N. Gavara, R. Farré, M. Rotger, D. Navajas, Probing mechanical properties of living cells by atomic force microscopy with blunted pyramidal cantilever tips, Phys. Rev. E. 72 (2005) 21914. http://link.aps.org/doi/10.1103/PhysRevE.72.021914.

[25] M. Lekka, D. Gil, K. Pogoda, J. Dulińska-Litewka, R. Jach, J. Gostek, O. Klymenko, S. Prauzner-Bechcicki, Z. Stachura, J. Wiltowska-Zuber, K. Okoń, P. Laidler, Cancer cell detection in tissue sections using AFM., Arch Biochem Biophys. (2012). doi:10.1016/j.abb.2011.12.013.

[26] M. Plodinec, Probing the determinants of cellular elasticity by AFM [Ph.D.], (2012).

[27] J.E. Sader, I. Larson, P. Mulvaney, L.R. White, Method for the calibration of atomic force microscope cantilevers, Rev. Sci. Instrum. 66 (1995) 3789–3798. doi:doi:http://dx.doi.org/10.1063/1.1145439.

[28] M.W. Tibbitt, K.S. Anseth, Hydrogels as extracellular matrix mimics for 3D cell culture, Biotechnol. Bioeng. (2009). doi:10.1002/bit.22361.

[29] A. Sawhney, C. Pathak, J. Hubbell, Bioerodible hydrogels based on photopolymerized poly (ethylene glycol)-co-poly (alpha-hydroxy acid) diacrylate macromers, Macromolecules. (1993). doi:10.1021/ma00056a005.

[30] M.P. Lutolf, Integration column: Artificial ECM: expanding the cell biology toolbox in 3D, Integr. Biol. (2009). doi:10.1039/b902243k.

[31] J.H. Hoh, C. Schoenenberger, Surface morphology and mechanical properties of MDCK monolayers by atomic force microscopy, J. Cell Sci. (1994).

[32] E.-Y. Kwon, Y.-T. Kim, D.-E. Kim, Investigation of penetration force of living cell using an atomic force microscope, J. Mech. Sci. Technol. 23 (2009) 1932–1938. doi:10.1007/s12206-009-0508-z.

[33] K.L. Bagnoli, Influence of EGF on HaCaT Cells as Measured by AFM with a Comparision of AFM and 3D Optical Deconvolution Using MH-S Cells, University of Connecticut, 2007.

[34] K. Gelse, E. Pöschl, T. Aigner, Collagens - Structure, function, and biosynthesis, Adv. Drug Deliv. Rev. (2003). doi:10.1016/j.addr.2003.08.002.

[35] W.S. Leong, C.Y. Tay, H. Yu, A. Li, S.C. Wu, D.H. Duc, C.T. Lim, L.P. Tan, Thickness sensing of hMSCs on collagen gel directs stem cell fate, Biochem. Biophys. Res. Commun. (2010). doi:10.1016/j.bbrc.2010.09.052.

[36] J.P. Winer, S. Oake, P.A. Janmey, Non-linear elasticity of extracellular matrices enables contractile cells to communicate local position and orientation, PLoS One. (2009). doi:10.1371/journal.pone.0006382.

[37] Y.L. Yang, L.M. Leone, L.J. Kaufman, Elastic moduli of collagen gels can be predicted from two-dimensional confocal microscopy, Biophys. J. (2009). doi:10.1016/j.bpj.2009.07.035.

[38] A.J. Heim, W.G. Matthews, T.J. Koob, Determination of the elastic modulus of native collagen fibrils via radial indentation, Appl. Phys. Lett. (2006). doi:10.1063/1.2367660.

[39] X. Ma, M.E. Schickel, M.D. Stevenson, A.L. Sarang-Sieminski, K.J. Gooch, S.N. Ghadiali, R.T. Hart, Fibers in the Extracellular Matrix Enable Long-Range Stress Transmission between Cells, Biophys. J. 104 (2013) 1410–1418. doi:http://dx.doi.org/10.1016/j.bpj.2013.02.017.

[40] M.P. Wenger, L. Bozec, M.A. Horton, P. Mesquida, Mechanical properties of collagen fibrils, Biophys J. (2007). doi:S0006-3495(07)71383-8 [pii]\n10.1529/biophysj.106.103192.

[41] S. Bancelin, C. Aimé, I. Gusachenko, L. Kowalczuk, G. Latour, T. Coradin, M.-C. Schanne-Klein, Determination of collagen fibril size via absolute measurements of second-harmonic generation signals, Nat. Commun. 5 (2014) 4920.

[42] T. USHIKI, Collagen Fibers, Reticular Fibers and Elastic Fibers. A Comprehensive Understanding from a Morphological Viewpoint, Arch. Histol. Cytol. 65 (2002) 109–126. doi:10.1679/aohc.65.109.

[43] B.A. Roeder, K. Kokini, J.E. Sturgis, J.P. Robinson, S.L. Voytik-Harbin, Tensile Mechanical Properties of Three-Dimensional Type I Collagen Extracellular Matrices With Varied Microstructure, J. Biomech. Eng. (2002). doi:10.1115/1.1449904.

[44] P.D. Yurchenco, B.L. Patton, Developmental and pathogenic mechanisms of basement membrane assembly, Curr. Pharm. Des. (2009).

[45] P.D. Yurchenco, J.C. Schittny, Molecular architecture of basement membranes, FASEB J. (1990).

[46] J. Takagi, Y. Yang, J. Liu, J. Wang, T.A. Springer, Complex between nidogen and laminin fragments reveals a paradigmatic β-propeller interface, Nature. (2003).

doi:10.1038/nature01873.

[47] R. Kalluri, Angiogenesis: Basement membranes: structure, assembly and role in tumour angiogenesis, Nat. Rev. Cancer. (2003). doi:10.1038/nrc1094.

[48] E. Pöschl, U. Schlötzer-Schrehardt, B. Brachvogel, K. Saito, Y. Ninomiya, U. Mayer, Collagen IV is essential for basement membrane stability but dispensable for initiation of its assembly during early development, Development. 131 (2004) 1619 LP-1628. http://dev.biologists.org/content/131/7/1619.abstract.

[49] T.T. Goodman, P.L. Olive, S.H. Pun, Increased nanoparticle penetration in collagenase-treated multicellular spheroids., Int. J. Nanomedicine. (2007).

[50] B. Glimelius, B. Norling, T. Nederman, J. Carlsson, Extracellular matrices in multicellular spheroids of human glioma origin: increased incorporation of proteoglycans and fibronectin as compared to monolayer cultures, Apmis. (1988).

[51] M.J. Paszek, N. Zahir, K.R. Johnson, J.N. Lakins, G.I. Rozenberg, A. Gefen, C.A. Reinhart-King, S.S. Margulies, M. Dembo, D. Boettiger, D.A. Hammer, V.M. Weaver, Tensional homeostasis and the malignant phenotype, Cancer Cell. 8 (2005) 241–254. doi:10.1016/j.ccr.2005.08.010.

[52] P.P. Provenzano, D.R. Inman, K.W. Eliceiri, P.J. Keely, Matrix density-induced mechanoregulation of breast cell phenotype, signaling and gene expression through a FAK-ERK linkage, Oncogene. 28 (2009) 4326–4343. http://dx.doi.org/10.1038/onc.2009.299.

[53] O. Chaudhuri, S.T. Koshy, C. Branco da Cunha, J.-W. Shin, C.S. Verbeke, K.H. Allison, D.J. Mooney, Extracellular matrix stiffness and composition jointly regulate the induction of malignant phenotypes in mammary epithelium, Nat Mater. 13 (2014) 970–978. http://dx.doi.org/10.1038/nmat4009.

[54] R. TIMPL, H. WIEDEMANN, V. VAN DELDEN, H. FURTHMAYR, K. KÜHN, A Network Model for the Organization of Type IV Collagen Molecules in Basement Membranes, Eur. J. Biochem. 120 (1981) 203–211. doi:10.1111/j.1432-1033.1981.tb05690.x.

[55] K. Kühn, H. Wiedemann, R. Timpl, J. Risteli, H. Dieringer, T. Voss, R.W. Glanville, Macromolecular structure of basement membrane collagens, FEBS Lett. 125 (1981) 123–128. doi:http://dx.doi.org/10.1016/0014-5793(81)81012-5.

[56] F. Pampaloni, E.G. Reynaud, E.H.K. Stelzer, The third dimension bridges the gap between cell culture and live tissue, Nat. Rev. Mol. Cell Biol. 8 (2007) 839–845. http://dx.doi.org/10.1038/nrm2236.

Figure Captions

Figure 1. (a) Sketch shows stepwise fitting of Sneddon's model into force curve data which gets converted into modulus vs. indentation curve. Modulus data from each pixel is plotted as stiffness map at various depths. (b) Indentation modulus profile of MCS-1 upto depth of 80 nm. Scan area of 20 x 20 μm having 64 x 64 pixels. (c) Illustration explaining various nanomechanical features visible in stiffness profile. Large central green colored region is ECM in between cells and cells embedded in the matrix are colored red.

Figure 2. Stiffness maps of sample MCS-1 at various depths (a) At depth of 280 nm, modulus of ECM is at 10 kPa and cells have stiffness < 100 kPa. Double red arrows mark interconnecting collagen type I stress fiber. (b) Modulus of cell membrane and ECM interface at depth of 800 nm is marked by double green arrows, has stiffness greater than 316 kPa, hence observed as string of black pixels. (c) Double green arrows mark regions of high stiffness at cell membrane-ECM interface at 1 μm depth. (d) At 1.35 μm depth, cell embedded deep inside the ECM can be observed with stiffness > 31.6 kPa is marked by dotted red square.

Figure 3. Sketch describes three types of nanomechanical topographies identified with DDIP. Type (A) are long range collagen type I stress fibers. They have considerable high stiffness as compared with surrounding ECM. Type (B) are identified as regions of high stiffness at interface of cell membrane and ECM. Type (C) are cells embedded deep inside the ECM. They are identified by gradual increase of stiffness as AFM probe indents deeper into the ECM.

Figure 4. Standard deviation of calculated modulus is shown as percentage error maps at various depths (a) Error profile of stiffness upto depth of 80 nm. ECM has higher percentile error as compared to cells forming MCS. (b) At 500 nm depth error is < 1 for both cells and ECM. (c) Probe indents deeper at depth of 1 μm. Edge of the cell

interacting with ECM has higher error. Region of cell membrane – ECM interface is marked by two green arrows has percentile error > 1.

Figure 5. DDIP of sample MCS-2 at various depths. Sketch (a) shows various nanomechanical features visible in indentation profile of the sample. At depth of 0.17 μm (b) cell lodged inside the ECM can be observed on top right corner. High stiffness at cell membrane –ECM interface is marked by green arrow. Type I Collagen fiber at 0.49 μm (c) can be recognized by long stretch of black pixels having stiffness > 316 kPa. The fiber is marked by red arrow. Modulus of both ECM and cell is centered around 10 kPa at depths of 0.8 μm (e), 1 μm (f) and 1.44 μm (g). There is gradual decrease of stiffness at cell membrane – ECM interface from 316 kPa to 31.6 kPa from depth of 0.17 μm to 1.44 μm.

Figures

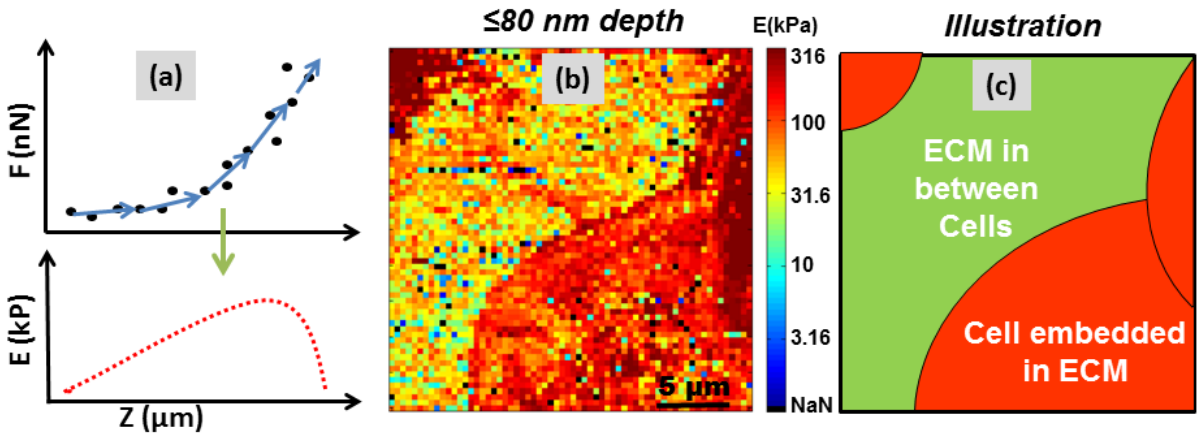

Figure 1.

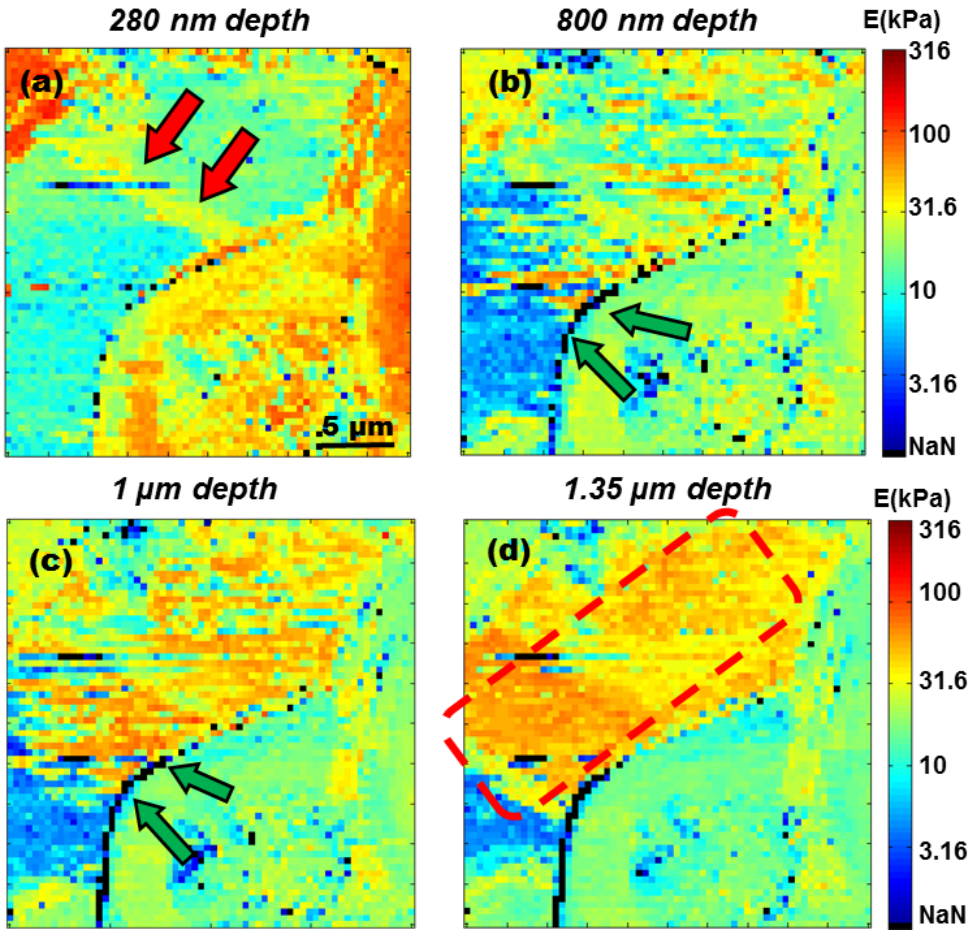
280 nm depth
800 nm depth
E(kPa)
316
100
31.6
10
3.16
NaN
(a)
(b)
5 µm
1 µm depth
1.35 µm depth
E(kPa)
316
100
31.6
10
3.16
NaN
(c)
(d)

Figure 2.

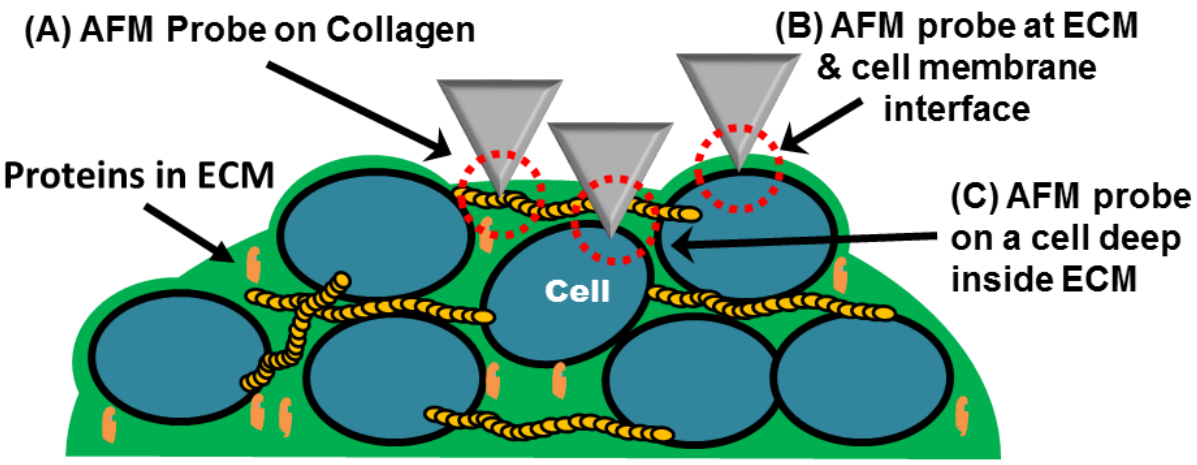
(A) AFM Probe on Collagen
(B) AFM probe at ECM & cell membrane interface
Proteins in ECM
(C) AFM probe on a cell deep inside ECM
Cell

Figure 3.

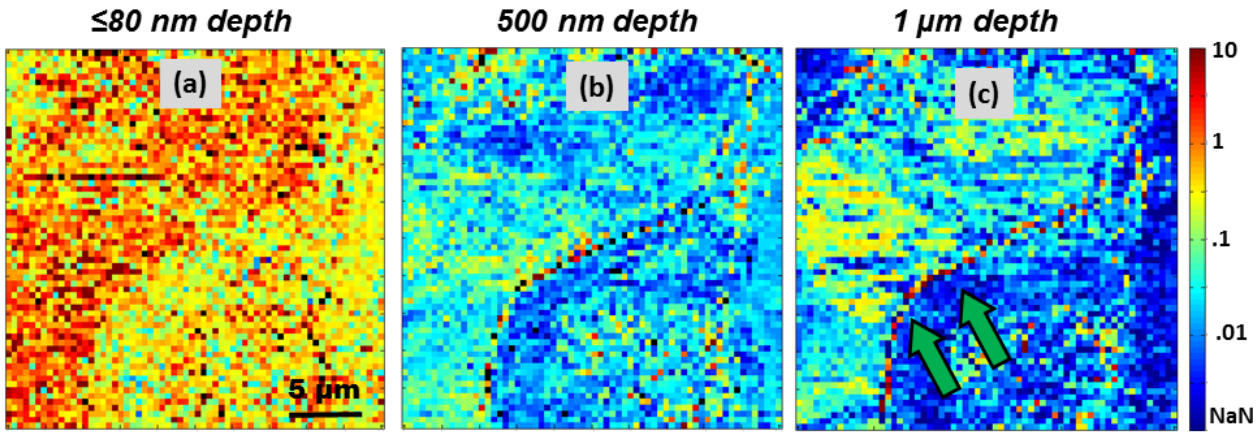

Figure 4.

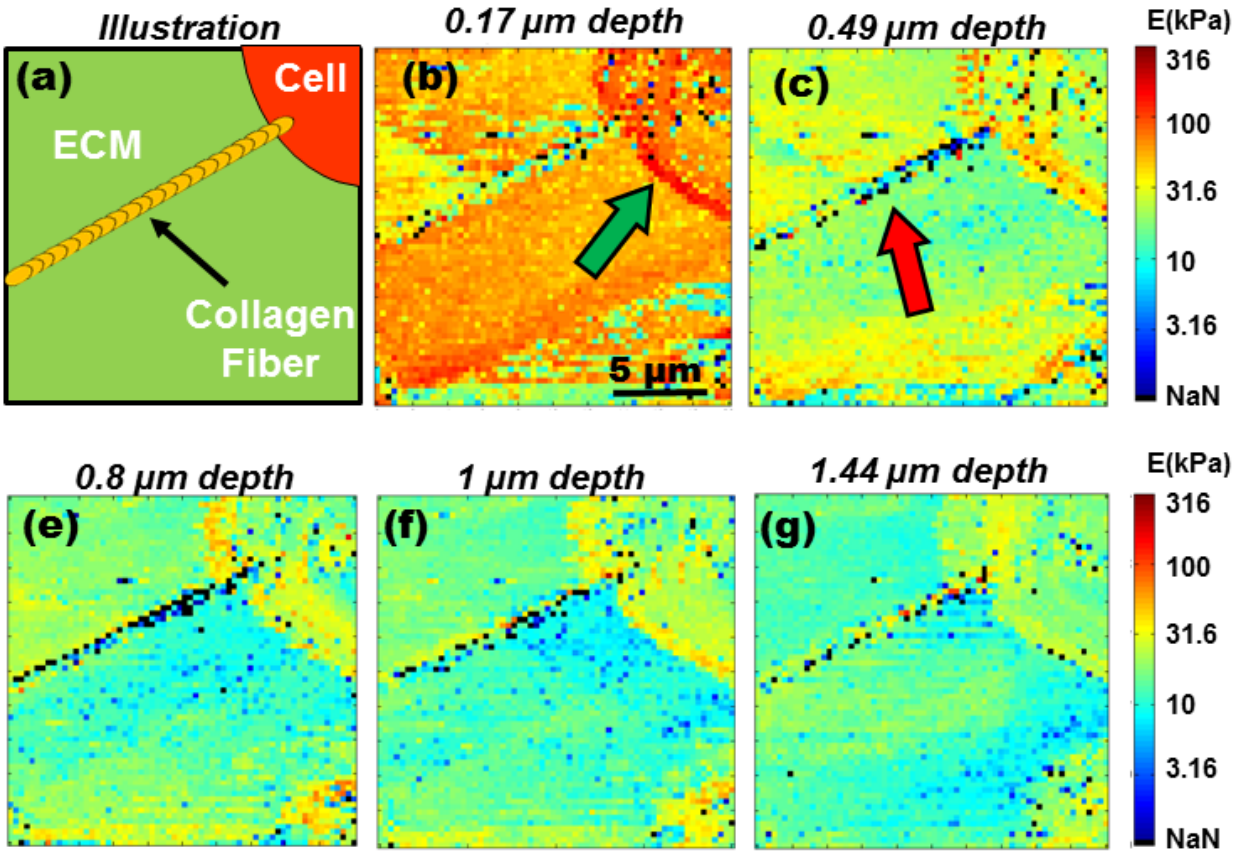
Illustration
(a)
Cell
ECM
Collagen
Fiber
0.17 μm depth
(b)
5 μm
0.49 μm depth
(c)
E(kPa)
316
100
31.6
10
3.16
NaN
0.8 μm depth
(e)
1 μm depth
(f)
1.44 μm depth
(g)
E(kPa)
316
100
31.6
10
3.16
NaN

Figure 5.